Morphology evolution during the growth of strained-layer superlattices

L. E. Shilkrot,[1] D. J. Srolovitz,[2] and J. Tersoff[3]
[1]*Division of Engineering, Brown University, Providence, Rhode Island 02912*
[2]*Princeton Materials Institute and Department of Mechanical & Aerospace Engineering, Princeton University, Princeton, New Jersey 08540*
[3]*IBM Research Division, Thomas J. Watson Research Center, Yorktown Heights, New York 10598*
(Received 13 March 2000)

We present a linear stability analysis for epitaxial growth of strained-layer superlattices, calculating how a shape perturbation propagates through the whole multilayer stack. We assume that bulk diffusion is negligible, so the morphology is controlled by surface diffusion. Unlike the case of a single strained layer, there are conditions under which the growth of the planar superlattice is stable, i.e., perturbations to the growth surface decay. For the conditions of unstable film growth (where the amplitude of the perturbation increases from layer to layer), we find three different types of resulting film morphology, classified according to the phase of the perturbation in successive layers, which is a function of materials parameters and growth conditions. We also determine the growth rate and wave vector of the propagating perturbation corresponding to the fastest growing instability wave.

I. INTRODUCTION

Semiconductor superlattices are in widespread use in a number of modern optoelectronic applications. Magnetic multilayers possessing giant magnetoresistance are playing an increasing role in magnetic and magneto-optic storage technologies. The introduction of artificial periodicities, by repeating a pattern of layers of different materials, modifies the electronic band structure and electron transport properties, thereby providing an approach to fine-tune materials properties.

For most applications, the ideal superlattice consists of a periodic array of uniform, distinct layers separated by sharp, atomically flat, coherent interfaces. However, misfit stress causes deviations from this ideal structure, due to plastic (misfit dislocation formation) or elastic relaxation, which commonly occurs during the growth process. Recent progress has been made in incorporating misfitting materials into a superlattice. A very successful approach to cope with misfit dislocation formation is to grow the multilayer structure with a zero net misfit strain, i.e., with balanced alternating layers of tensile and compressive strain. By keeping the thickness of each individual layer in the superstructure below its critical thickness, the multilayer film grows dislocation-free.[1–3]

The origin of elastically driven relaxations in a multilayer film lies in the instability of a film under stress with respect to the formation of shape perturbations.[4–6] As each layer of material composing the multilayer film is deposited, the growing surface of the films develops an undulating profile. In the case of single-layer films, there is extensive experimental evidence[7–9] of this phenomenon. As more layers are deposited, undulated surfaces become buried under subsequent layers of materials, resulting in wavy interfaces. The resulting structure becomes modulated morphologically and, possibly, compositionally, as explained below.[10–15] If carefully controlled, these modulations may be exploited to form self-organizing quantum nanostructures,[16–19] which are potential candidates for semiconductor lasers due to their δ-function-like density of electronic states.

Eliminating elastically driven relaxations in the film is a challenging task, as this type of structural defect is caused by the presence of misfit stresses in the film, which is independent of the growth conditions. In this paper, we examine the evolution of interface morphology during the growth of periodic, multilayer strained films. As shown below, a rich variety of interface morphologies may be obtained, depending on the properties of the materials making up the individual layers and on the growth conditions. In particular, planar layers can be stabilized against morphological perturbations.

Modulation of microstructure and composition during epitaxial growth is by no means a novel subject. Morphological instabilities in strained films have been studied in a continuum model[4–6,20] and in a step-flow model by Tersoff.[21] In alloys, coupled morphological and composition modulations can lead to a rich behavior.[21–24] In some cases, spinodal decomposition or compositional stresses can drive a compositional instability, which in turn modulates the morphology.[25,26]

Morphological modulations in multilayer films may cause lateral modulation of the vertically averaged composition. Such ''lateral composition modulations'' [10,11,14] have generated considerable interest. It is not clear that actual changes in local composition play a key role in the phenomenon, however. Rather, they appear to be closely related to the morphological modulations studied here.

In this paper, we present a simple model for the formation of modulated multilayer structures which does not rely on alloy decomposition processes. Instead, modulations occur in the layer thicknesses, which may be viewed as modulations of the vertically averaged composition, without the need for any change in the composition of the individual layers. We show that the competition between surface and elastic energy effects can lead to periodic interface modulations. Under certain conditions, these interface modulations can produce an overall lateral composition modulation in the growing

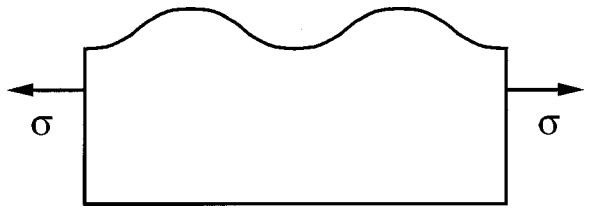

FIG. 1. A thin film with an undulating surface subjected to a stress σ. For a film in tension, as in this figure, the atomic planes are farther apart from one another in the troughs (the film is more stretched than average) and closer to one another at the crests.

multilayer film. Our analysis predicts the materials properties and growth conditions required to produce such modulations and both the wavelength and rate of growth of these modulations. We also predict the materials properties and growth conditions necessary to grow multilayer films which are stable against interface modulations. The existence of conditions for which films grow stably (i.e., with flat interfaces) is surprising since misfitting monolithic films are always unstable against surface modulations.

II. PROBLEM FORMULATION

Interface undulations in multilayer films are closely related to the well-known elastic instability of free surfaces of stressed solids.[4–6] Consider a thin film grown heteroepitaxially on a substrate, such that a misfit stress exists. If the surface is not flat, the stresses within the film are nonuniform. The nonuniform elastic energy along the surface causes a variation in chemical potential along the surface that can be relaxed by mass flow along the surface (i.e., surface diffusion). In the case of a sinusoidal perturbation,[6] these fluxes will result in the increase of the perturbation amplitude for any perturbation wavelength. The existence of nonnegative surface energy impedes the growth of these perturbations. The interplay between these two factors determines whether the perturbation amplitude will grow and, if so, the rate of growth. Short-wavelength perturbations decay, whereas long-wave modes grow exponentially with time.

If the surface of the film undulates (see Fig. 1), the atomic planes in the film are distorted by the nonuniform stress at the surface of the film. The average misfit stress in the film is denoted as σ and, for the sake of this argument, the lattice parameter of the film is originally smaller than that of the substrate (i.e., the misfit is negative and the film is in tension) and σ is positive. An elastic solution[6] shows that this film is more stretched in the troughs and more compressed at the crests of the free surface (Fig. 1). Consider now a situation in which a second film is deposited on the first with a lattice parameter which is greater than that of the substrate. In this case, the atoms of the second film will have lower energy if they sit in the troughs compared with sitting on the crests. As more material is added to the second film, the amplitude of the surface perturbation gets smaller and will eventually reverse such that the second film will have troughs above the crests in the first layer and vice versa. As additional layers grow, this perturbation may propagate through the entire stack of layers, either increasing or decreasing in amplitude and with the perturbations on adjacent layers either in or out of phase.

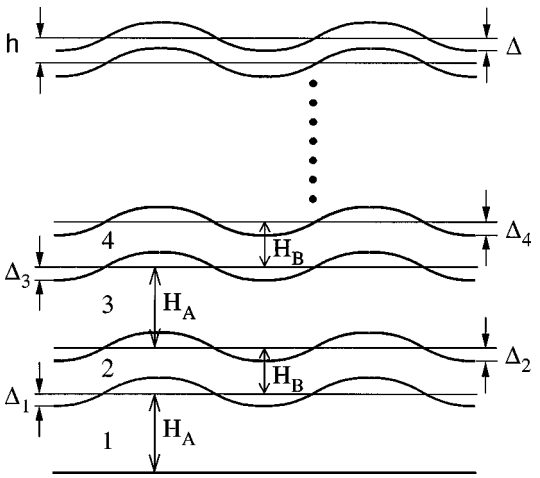

FIG. 2. A schematic illustration of the multilayer film geometry, indicating the amplitude of the interface undulations Δ and the layer thicknesses H. The odd-numbered layers correspond to material A and the even-numbered ones to material B.

We now formulate the problem in terms of continuum elasticity. Consider the multilayer film geometry presented in Fig. 2, which consists of alternating layers of two materials (materials A and B) epitaxially deposited on a substrate (material C). The interfaces between adjoining layers are assumed to be coherent. Effects due to the interfacial stresses associated with the buried interfaces[27] are explicitly neglected in this analysis. If the layers are misfitting with respect to the substrate, they may develop a morphological perturbation on the growing free surface, as discussed above. This surface perturbation will become a buried interface as more layers are deposited on top of it. This perturbed interface bounding misfitting materials will act as a source of stress and modify the stress field throughout the film and, especially, on the new growth surface. Each buried interface will affect the chemical potential on the surface and, therefore, will modify the surface diffusion and subsequently the surface profile.

We adopt the following notation for the remainder of the paper. All quantities related to layer k will have a subscript k. Thus, the thickness of growing layer k is denoted as h_k and that of the fully grown layer is denoted as H_k. H_k is equal to H_A for odd-numbered layers and H_B for even-numbered ones. The misfit stress in layer k is denoted as Σ_k and is equal to Σ_A for odd-numbered layers and Σ_B for even-numbered ones. Similarly, the amplitude of the perturbation to the surface of layer k is denoted as Δ_k. The present analysis is performed in the two spatial dimensions containing the substrate and substrate normal.

The thickness of the growing film $\bar{h}$ at time t can be written as

$$\bar{h}(t)=\sum_{j=1}^{k-1} H_j + h_k(t), \tag{1}$$

where layers up to $k-1$ are fully grown and have thickness H_j, respectively, and layer k is currently growing (i.e., it has not yet grown to thickness H_k). The average layer thickness, h_k, is always measured from the average height of the previous layer, such that the film profile is described by

$$h(x,t)=\overline{h}(t)+\Delta_k(x,t), \tag{2}$$

where $\Delta_k(x,t)$ is the perturbation to the growing surface of layer k.

In the simple model for film growth adopted in the present paper, each layer is deposited with a uniform rate r_k (r_A or r_B for A and B layers, respectively). The material is allowed to diffuse only along the growing surface. Without bulk diffusion, no morphology evolution occurs below the current growth surface. Mathematically, we write the evolution equation for the growing surface as[28]

$$\frac{\partial h}{\partial t}=r_k+\frac{D_k\Omega_k\theta_k}{k_BT}\frac{\partial^2\mu_k^s}{\partial s^2}, \tag{3}$$

where D_k is the surface diffusivity of the material of layer k, k_B is the Boltzmann constant, and Ω_k and θ_k are the atomic volume and surface atomic density, respectively. The chemical potential of the atoms at the surface of the growing layer μ_k^s and its second derivative are evaluated along the surface. This expression explicitly assumes that the deposition rate on each point of the surface is constant and unaffected by variations in the surface chemical potential.

The linear stability of the multilayer morphology is analyzed by considering a sinusoidal perturbation to the profile of an otherwise flat interface. We Fourier-transform the coordinate parallel to the substrate and denote the corresponding wave vector as ξ. Since this is done throughout, we will write $\Delta_k(\xi)$ simply as Δ_k. The present analysis is performed only to first order in perturbation theory, where the small parameter is the product of the wave vector ξ and the amplitude of the shape perturbation of a layer Δ. Within this approximation, the derivative along the surface in Eq. (3) is replaced by the derivative with respect to the x coordinate. Equation (3) may, therefore, be rewritten as

$$\frac{\partial\Delta_k}{\partial t}=-\xi^2\frac{D_k\Omega_k\theta_k}{k_BT}\mu_k^s(\xi). \tag{4}$$

Following Refs. 4 and 6, we write the chemical potential at the surface as

$$\mu(x)=\mu_0+\gamma_k\Omega_k\kappa(x)+\frac{\Omega_k}{2}\boldsymbol{\sigma}_k^s(x)\mathbf{S}\boldsymbol{\sigma}_k^s(x), \tag{5}$$

where μ_0 is the chemical potential of a flat surface bounding unstressed material and the other two terms in this expression are the surface energy and elastic contributions, respectively. $\kappa(x)$ is the curvature of the growing surface and γ_k is the surface energy of layer k. $\boldsymbol{\sigma}_k^s(x)$ is the stress tensor evaluated at the surface and $\mathbf{S}$ is the elastic compliance tensor of layer k. For the sake of simplicity, we also assume that the elastic constants of materials A and B are identical.

To first order in perturbation theory, the surface tension term in Eq. (5) can be written as $\mu_\gamma(\xi)=\gamma_k\Omega_k\kappa(\xi)=\gamma_k\Omega_k\xi^2\Delta_k$. The leading-order contribution to the elastic term in the chemical potential is associated with the coupling between the uniform misfit stress Σ and the nonuniform contribution to the stress tensor $\boldsymbol{\sigma}_k^s(x)$. Since the surface is nearly flat, the only term that enters the elastic contribution to the chemical potential is the normal stress parallel to the surface $\boldsymbol{\sigma}_{xx}^s(x)$, i.e., $\mu_{\rm el}(x)=\Omega_k\Sigma_k\boldsymbol{\sigma}_{xx}^s(x)/M$, where M is the elastic modulus in the direction along the surface which, in the plane strain approximation, is $E/(1-\nu^2)$, where E and ν are Young's modulus and the Poisson ratio, respectively. In the following, we derive an equation for the stress at the growing surface and assemble all of the terms in the evolution equation [Eq. (4)]. Next, we nondimensionalize this equation and analytically solve for the amplitude of the perturbation of the growing layer $\Delta_k(\xi)$ as a function of material parameters and growth conditions.

III. ELASTIC ANALYSIS

In this section, we determine the tangential component of the stress at the surface of the growing layer k in the multilayer structure. This stress is required to evaluate the elastic component of the chemical potential, as described above. We analyze this problem within the framework of two-dimensional, isotropic, plane strain elasticity, in which materials A and B have the same elastic constants. Elastic anisotropy does, however, appear to play an important role in some cases[20,29,30] and would make an interesting extension to the present work.

A simple analysis shows that there are two contributions to the stress $\boldsymbol{\sigma}_{xx}^s(x)$ in first order in perturbation theory,

$$\sigma_{xx}^s(x)=\sigma_{\rm surf}(x)+\sigma_{\rm int}(x). \tag{6}$$

The first term is associated with the surface itself and is present because the growing surface is not flat. This stress is the correction to the uniform misfit stress Σ_k (i.e., the xx component) that arises from the requirement that the surface tractions must be zero, as described by Asaro and Tiller,[4] Grinfeld,[5] Srolovitz,[6] and others. The Fourier transform of $\sigma_{\rm surf}(x)$ may be written as $\sigma_{\rm surf}(\xi)=-2|\xi|\Delta_k\Sigma_k$, where $|\xi|$ is the absolute value of the wave vector ξ and Δ_k is in Fourier space.

The second contribution to the stress at the surface in Eq. (6) is associated with the presence of buried interfaces and is only present when those interfaces are not flat. Because materials A and B have identical elastic constants, each interface contributes separately to the term $\sigma_{\rm int}$. We determine $\sigma_{\rm int}$ using the Eshelby procedure[31] for the stress created by a misfitting inclusion. Consider the nonflat interface between layers n and $n+1$, the shape of which is determined by the amplitude of the nth perturbation $\Delta_k(x)$ or, in Fourier space, $\Delta_n(\xi)$. If we make an imaginary cut along this interface, the macroscopic misfit stresses Σ_n and Σ_{n+1} create surface tractions along both sides of the cut. To balance these tractions, we apply equal and opposite corrective tractions along the surfaces of the cut and then ''weld'' the two pieces back together. The stress produced by these corrective tractions, evaluated at the free surface, is $\sigma_{\rm int}$ for the $n/n+1$ interface.

The tractions along the interface cut are, to first order in the small parameter $\Delta_n\xi_n$, the sum of the products of the misfit stresses Σ_n and Σ_{n+1} and the outer normals to the interface. In Fourier space, this traction $\mathbf{T}$ is

$$\mathbf{T}_x=-i\Delta_n\xi(\Sigma_n-\Sigma_{n+1}) \quad \text{and} \quad \mathbf{T}_y=\mathbf{0}, \tag{7}$$

i.e., only the tangential component of the tractions is present. We also make use of the fact that $\Delta_m\xi_m$ is small to replace the actual curved interface with a flat interface while keeping

the corrective tractions along that interface ($\mathbf{T}_c = -\mathbf{T}$) associated with the original curved interface. This line traction is parallel to and some distance from the free (growing) surface in an elastic half-plane. The expression for the stress field produced by such a line traction can be easily obtained by deriving the stresses produced by this traction in the whole elastic plane using the elastic Green's function[32] and applying a corrective solution to satisfy the boundary conditions at the free surface. The resultant expression is

$$\sigma_{\mathrm{int}}^{n/n+1} = -\Delta_n |\xi| (\Sigma_n - \Sigma_{n+1}) \left[2 - \frac{|\xi| h_{nk}}{1-\nu} \right] \exp(-|\xi| h_{nk}). \tag{8}$$

In order to determine the stress on the surface from all interfaces, this expression must be summed over n. The distance h_{nk} in this equation is the distance from the interface under consideration to the growing surface:

$$h_{nk} = \sum_{j=n+1}^{k-1} H_j + h_k. \tag{9}$$

Note that this stress is time-dependent, since the thickness of the growing layer h_k increases linearly for a fixed growth rate r_k as $h_k = r_k t$.

Equations (4)–(6) provide the necessary framework to write down the equation governing the amplitude of the perturbation to the growing layer k. Inserting Eqs. (5)–(9) into Eq. (4) yields

$$\frac{\partial \Delta_k}{\partial h_k} = \frac{D_k \Omega_k^2 \theta_k}{r_k k_B T} |\xi|^3 \left\{ -\gamma_k |\xi| \Delta_k + 2 \frac{\Sigma_k^2}{M} \Delta_k - \frac{\Sigma_k}{M} \left(\sum_{j=1}^{k-1} \Delta_j (\Sigma_{j+1} - \Sigma_j) \left[2 - \frac{|\xi| h_{jk}}{1-\nu} \right] e^{-|\xi| h_{jk}} \right) \right\}, \tag{10}$$

where we have replaced the variable time with the thickness of the growing layer h_k. The amplitude of the perturbation to the surface of each layer is a function of the amplitude of the perturbations to the interfaces of all underlying layers.

If we remove the terms in Eq. (10) associated with the buried interfaces, we find that it is identical to that derived by Asaro and Tiller[4] and Srolovitz[6] in the context of the analysis of the stability of a free surface bounding a stressed body. They found that there exists a wave vector for which a sinusoidal shape perturbation grows the fastest. We denote this wave vector for material A as $\xi_A = (3\Sigma_A^2)/(2M\gamma_A)$ and use it as a length scale throughout the remainder of this analysis. We introduce the ratio of the misfit stress in material B (even-numbered layers) to that in material A (odd-numbered layers) $\beta = \Sigma_B / \Sigma_A$ and the ratio of surface energies $\Gamma = \gamma_B / \gamma_A$. The difference between the misfit stresses in the adjacent layers n and $n+1$ is $\Sigma_{n+1} - \Sigma_n = (-1)^n \Sigma_A (1-\beta)$.

We consider the evolution of odd-numbered layers separately from the even-numbered layers. Equation (10) becomes

$$\frac{\partial \Delta_k}{\partial h_k^*} = \Phi_A \xi^{*3} \left[(2 - \tfrac{3}{2}\xi^*) \Delta_k - \sum_{j=1}^{k-1} (-1)^j \Delta_j (1-\beta) \times \left(2 - \frac{\xi^* h_{jk}^*}{1-\nu} \right) e^{-\xi^* h_{jk}^*} \right] \tag{11a}$$

for odd-numbered layers and

$$\frac{\partial \Delta_k}{\partial h_k^*} = \Phi_B \xi^{*3} \left[(2\beta^2 - 3/2\Gamma\xi^*) \Delta_k - \sum_{j=1}^{k-1} (-1)^j \Delta_j \beta (1-\beta) \times \left(2 - \frac{\xi^* h_{jk}^*}{1-\nu} \right) e^{-\xi^* h_{jk}^*} \right] \tag{11b}$$

for even-numbered layers. Here, the dimensionless wave vector ξ^* is measured in terms of ξ_A, $\xi^* = |\xi| / \xi_A$, and the parameters Φ_A and Φ_B are defined as $\Phi_A = (D_A \Omega_A^2 \theta_A \Sigma_A^2 \xi_A^2)/(r_A k_B T M)$ and $\Phi_B = (D_B \Omega_B^2 \theta_B \Sigma_A^2 \xi_A^2)/(r_B k_B T M)$, respectively. The thicknesses of each layer are also made dimensionless, as follows: $H_k \xi_A = H_k^*$, $H_A \xi_A = H_A^*$, $H_B \xi_A = H_B^*$, $h_{jk} \xi_A = h_{jk}^*$, and $h_k \xi_A = h_k^*$.

IV. SOLUTION OF THE EVOLUTION EQUATION

In order to determine the temporal evolution of the amplitude of the perturbation on the surface of the growing film, we must integrate the evolution equation [Eq. (11)] over the entire layer thickness (i.e., from $h_k = 0$ to $h_k = H_k$), starting from the initial condition $\Delta_k(0) = \Delta_{k-1}(H_{k-1})$. Equation (11) can be simplified by the introduction of new variables:

$$X_j = \Delta_j \exp\left(\xi^* \sum_{n=2}^{j} H_n^* \right). \tag{12}$$

The evolution equation now becomes

$$\frac{\partial X_k}{\partial h_k^*} = \Phi_A \xi^{*3} \left[(2 - \tfrac{3}{2}\xi^*) X_k - e^{\xi^* H_A^*} \sum_{j=1}^{k-1} (-1)^j X_j (1-\beta) \left(2 - \frac{\xi^* h_{jk}^*}{1-\nu} \right) e^{-\xi^* h_k^*} \right] \tag{13a}$$

for odd-numbered layers and

$$\frac{\partial X_k}{\partial h_k^*} = \Phi_B \xi^{*3} \left[(2\beta^2 - 3/2\Gamma\xi^*) X_k - e^{\xi^* H_B^*} \sum_{j=1}^{k-1} (-1)^j X_j \beta (1-\beta) \left(2 - \frac{\xi^* h_{jk}^*}{1-\nu} \right) e^{-\xi^* h_k^*} \right] \tag{13b}$$

for even-numbered layers with the initial condition modified accordingly.

Integration of Eq. (13) yields the following linear relations:

$$X_k = X_{k-1}F_A - \sum_{n=1}^{k-1}(-1)^n X_n(1-\beta) \times\left[\Xi_A + \Psi_A\left(\sum_{j=n+1}^{k-1} H_j^*\right)\right] \tag{14a}$$

for odd-numbered layers and

$$X_k = X_{k-1}F_B - \sum_{n=1}^{k-1}(-1)^n X_n\beta(1-\beta) \times\left[\Xi_B + \Psi_B\left(\sum_{j=n+1}^{k-1} H_j^*\right)\right] \tag{14b}$$

for even-numbered layers, where we have introduced the following composite parameters:

$$F_A = \exp(\Phi_A\delta_A\xi^{*3}H_A^*),$$

$$F_B = \exp(\Phi_B\delta_B\xi^{*3}H_B^*),$$

$$\Psi_A = -(F_A-1)\xi^*/[(1-\nu)\delta_A],$$

$$\Psi_B = -(F_B-1)\xi^*/[(1-\nu)\delta_B],$$

$$\Xi_A = \left(2-\frac{1}{(1-\nu)\Phi_A\xi^{*2}\delta_A}\right)\frac{F_A-1}{\delta_A} + \frac{\xi^*H_A^*}{\delta_A(1-\nu)},$$

$$\Xi_B = \left(2-\frac{1}{(1-\nu)\Phi_B\xi^{*2}\delta_B}\right)\frac{F_B-1}{\delta_B} + \frac{\xi^*H_B^*}{\delta_B(1-\nu)},$$

$$\delta_A = 1/(\Phi_A\xi^{*2}) + (2-3/2\xi^*),$$

and

$$\delta_B = 1/(\Phi_B\xi^{*2}) + (2\beta^2 - 3/2\Gamma\xi^*).$$

In order to improve the clarity of the results, we restrict consideration of the solutions to the special case (to be relaxed later) where materials A and B are identical in every respect, except that the magnitude of the misfit stress Σ with respect to the substrate is equal and opposite in the two materials (i.e., $\beta=-1$). To be specific, both materials have the same values of D, θ, Ω, and γ, and are grown with the same deposition rate r and to the same thickness H. Since the two materials have the same thickness and equal and opposite misfit, there will be no driving force to form misfit dislocations provided that each layer can be grown to a thickness H on the pristine substrate without dislocation formation. Equation (14) can now be rewritten without subscripts and with $\beta=-1$ and $\Gamma=1$:

$$X_k = X_{k-1}F - 2\sum_{j=1}^{k-1}(-1)^{k-j-1}X_j[\Psi H^*(k-j-1)+\Xi]. \tag{14'}$$

The variables can now be rewritten as $\xi_0 = 3\Sigma^2/(2M\gamma)$, $\xi^* = |\xi|/\xi_0$, $H\xi_0 = H^*$, $F = \exp(\Phi\delta\xi^{*3}H^*)$, $\Phi = (D\Omega^2\theta\Sigma^2\xi_0^2)/(rk_BTM)$, $\Psi = -(F-1)\xi^*/[(1-\nu)\delta]$, $\delta = 1/(\Phi\xi^{*2}) + (2-3/2\xi^*)$, and

$$\Xi = \left(2-\frac{1}{(1-\nu)\Phi\xi^{*2}\delta}\right)\frac{F-1}{\delta} + \frac{\xi^*H^*}{\delta(1-\nu)},$$

and Eq. (12) becomes

$$X_j = \Delta_j e^{\xi^*H^*(j-1)}. \tag{12'}$$

While the integrated equation for the evolution of the surface of the topmost layer [cf. Eq. (14′)] is a function of the amplitude of the perturbations to all buried interfaces, it can be reduced to a much simpler linear recurrence relation that only involves the amplitude of the perturbations on three previous, consecutive interfaces, as shown in detail in the Appendix. Since the recurrence relation is linear and only depends on the amplitudes of the perturbations to three consecutive interfaces, the solution ($k\geqslant 4$) can be rewritten in the following form:

$$\Delta_k^+ = \alpha_1\lambda_1^{k-1} + \alpha_2\lambda_2^{k-1} + \alpha_3\lambda_3^{k-1}, \tag{15}$$

where we normalize the amplitude of the interface perturbation for each layer Δ_k by that of the first layer Δ_1 (i.e., $\Delta_l^+ = \Delta_l/\Delta_1$). λ_1, λ_2, and λ_3 are the eigenvalues of the matrix $\mathbf{L}$ [Eq. (A5)],

$$\mathbf{L} = \begin{pmatrix} e^{-\xi^*H^*}(F-2-2\Xi) & 1 & 0 \\ e^{-2\xi^*H^*}(2F-1+2\Psi H^*-2\Xi) & 0 & 1 \\ e^{-3\xi^*H^*}F & 0 & 0 \end{pmatrix}, \tag{16}$$

and the coefficients α_1, α_2, and α_3 are the coefficient of the expansion of the vector $\mathbf{Y}_1$ in the basis of the eigenvectors of the matrix $\mathbf{L}$ (see the Appendix). The two elements of the vector $\mathbf{Y}_1$, which are the amplitudes of the perturbation of the interface above layers 2 and 3, $\mathbf{Y}_1 = \langle\Delta_3^+, \Delta_2^+, 1\rangle$, need to be computed directly using Eqs. (12′) and (14′).

Because the perturbation amplitude grows as the eigenvalues of $\mathbf{L}$ to a power equal to the number of layers minus one [see Eq. (15)] in the limit of a large number of layers, the amplitude of the perturbation on layer k is dominated by the largest eigenvalue:

$$\Delta_\lambda^+ = \alpha\lambda_1^{k-1}, \tag{17}$$

where λ_1 is the largest eigenvalue of $\mathbf{L}$ and α_1 is the corresponding expansion coefficient. In the case when the maximal eigenvalues form a complex-conjugate pair, the previous equation should include the complex-conjugate term as well (Δ_k^+ is a real number),

$$\Delta_k^+ = \alpha_1\lambda_1^{k-1} + \overline{\alpha}_1\overline{\lambda}_1^{k-1}. \tag{17'}$$

Here, the bar over the variable indicates complex conjugate.

This asymptotic regime is reached fairly quickly because the difference between the asymptotic equation [Eq. (17)] and the full equation [Eq. (15)] decays as a power of the ratio of the eigenvalues. Thus, in studying the stability of the multilayer film, we use Eq. (17) instead of the full equation [Eq. (15)] and the perturbation behavior is fully determined by the dependence of λ_{-1} on the parameters ξ^* (normalized wave vector), H^* (normalized thickness of an individual

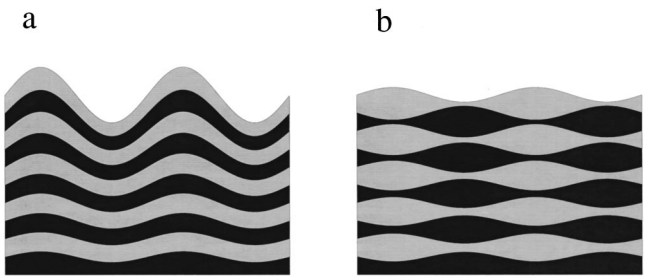

FIG. 3. Multilayer film morphology produced by (a) an in-phase instability and (b) an out-of-phase instability. In the latter case, the morphology modulation produces a net composition modulation in the direction parallel to the substrate.

layer), and Φ (see above). Large Φ results from fast diffusion or slow deposition, as discussed below.

Given a set of parameters H^* and Φ, as well as the magnitude of the wave vector ξ^*, the morphology of the multilayer structure can be classified according to the value of λ_1. If the absolute value of λ_1 is smaller than 1, the perturbation does not propagate through the multilayer film but, rather, decays after a few layers, i.e., the interfaces become flat and we refer to this structure as stable. In the opposite case, when the absolute value of λ_1 is greater than 1, the amplitude of the perturbation to the interfaces grows with the layer number. We refer to this structure as unstable. We can examine the nature of this instability by considering λ_1 in more detail.

The morphology of the structure in the unstable regime is determined by the complex phase of λ_1. If λ_1 is real and positive, the perturbation amplitudes (Δ) grows from interface to interface and the perturbations on consecutive interfaces will be in phase, as indicated schematically in Fig. 3(a). If λ_1 is real and negative, the value of Δ grows from interface to interface and perturbations on consecutive interfaces are out of phase, i.e., the amplitude of the perturbations changes sign at each interface (the layer is accordion-shaped) as shown in Fig. 3(b). The resulting structure is modulated, not only morphologically but also compositionally, since a vertical cross section of a multilayer film in the plane perpendicular to the plane of Fig. 3(b) will show oscillations in the fraction of materials A and B. When λ_1 is complex, the perturbations at consecutive interfaces are out of phase as well (i.e., peaks in one layer line up with either peaks or troughs in preceding layers), but the sign change is not regular and will be determined by the complex phase of λ_1. The in-phase and out-of-phase morphologies show some resemblance to the vertical correlations among stacked islands, discussed by Shchukin *et al.*[29]

We reiterate that the asymptotic equation [Eq. (17)] is valid provided that the expansion coefficient α_1, corresponding to the maximal eigenvalue λ_1, is not zero, and its value is not negligible compared to the expansion coefficients (α_2 and α_3) corresponding to the other two eigenvalues (λ_2 and λ_3). In the quantitative analysis of the results presented in the next section, we checked to insure that this condition is satisfied. We present our results in terms of the stability diagram, which provides a link between the materials and growth parameters and the morphology of the interfaces.

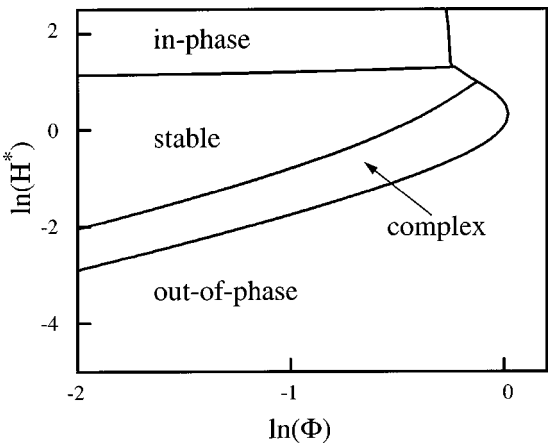

FIG. 4. Stability diagram for a growing multilayer film, indicating the types of morphologies expected classified according to the eigenvalue λ_{max}. In the region labeled stable, the film will exhibit flat interfaces. In the in-phase and out-of-phase regions, the interface perturbations grow with increasing thickness and are of the form shown in Figs. 3(a) and 3(b), respectively. The complex region is discussed in the text.

V. STABILITY DIAGRAMS

In this section, we examine the dependence of Δ on the material and growth parameters captured in Φ and H^* for the special case where adjacent layers are the same except for the misfit with respect to the substrate (i.e., the misfits are equal but have opposite sign). For each point in the Φ-H^* plane, we determine the dependence of the maximal eigenvalue λ_1 on the normalized eigenvector ξ^*. The rate at which the perturbations grow depends on the imposed perturbation wavelength. The fastest growing perturbation corresponds to $\lambda_1=\lambda_{max}$, which occurs at $\xi^*=\xi^*_{max}$. The nature of the evolution of the perturbation amplitude with layer number is determined by whether the magnitude of λ_{max} is greater or less than unity and whether it is real or complex, as discussed above. The resultant stability diagram is presented in Fig. 4. Four distinct fields are found on the stability diagram. The region corresponding to $|\lambda_{max}|<1$, marked stable in Fig. 4, indicates that the amplitude of the perturbations to the interfaces decreases with an increasing number of layers for all wavelengths. In the region of unstable growth ($|\lambda_{max}|>1$), the mode of the instability is determined by the phase of λ_{max} as discussed in the preceding section. For thick layers (large H^*) and slow diffusion (low Φ), the instability corresponds to in-phase growth, resulting in snakelike layers, as shown in Fig. 3(a). As Φ increases and/or the layers are thin, the interface perturbations grow out of phase, resulting in accordionlike layers, as shown schematically in Fig. 3(b). Between the unstable/out-of-phase and stable fields, a region of complex λ_{max} exists. In this region of the diagram, consecutive interfaces are either in or out of phase depending on the interface number. This pattern of in- and out-of-phase interfaces may be either periodic or aperiodic as determined by the complex phase of λ_{max}.

A contour plot of the logarithm of the absolute value of λ_{max} is shown in Fig. 5. The contour lines are drawn only in the region where the film growth is unstable, i.e., $|\lambda_{max}|>1$. The magnitude of λ_{max} and, consequently, the rate of growth

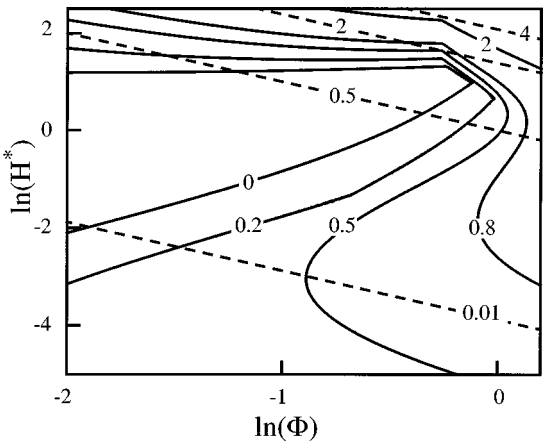

FIG. 5. Contour plot of the logarithm of the absolute value of λ_{max}. For comparison, dashed lines show the contours of the logarithm of λ_s, as for a single layer, as described in the text.

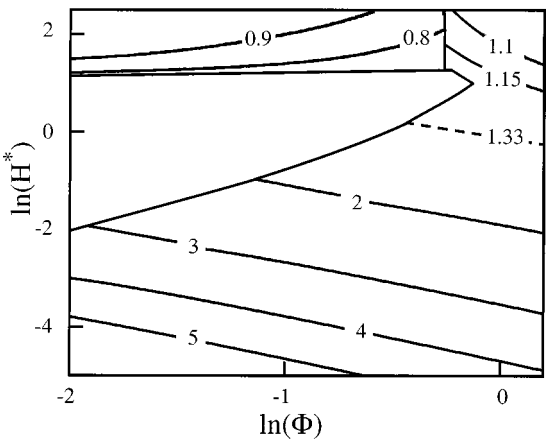

FIG. 6. Contour plot of ξ^*_{max} for the domains of unstable multilayer growth. For comparison, the dashed contour corresponds to $\xi^*_{max}=\frac{4}{3}$, the critical wave vector below which perturbations of a single layer are unstable.

of the instability increases with increasing distance from the stable growth domain within the Φ-H^* plane. In order to put the rate of growth of the instability into perspective, we compare the degree to which the amplitude of the instability changes during the growth of a single layer with that for growing either pure A or pure B on the substrate to the thickness of one layer. The latter can be found by integrating Eq. (10), omitting the contributions associated with the buried interfaces. The corresponding value which we define as λ_s is simply $\lambda_s=\exp(\Phi H^*/2)$. Contours of constant $\ln(\lambda_s)$ form straight lines in the Φ-H^* stability map of Fig. 5. The contours of constant $\ln(\lambda_{max})$ asymptotically approach the straight single-layer lines $[\ln(\lambda_s)]$ at large film thickness H^*. This is to be expected since the stress on the surface due to a buried interface decreases exponentially with the distance between the surface and buried layer [see Eq. (8)].

The magnitude of the wave vector of the most unstable perturbation ξ^*_{max} (corresponding to the eigenvalue λ_{max}) determines the overall film morphology. For a pure material (i.e., single-layer film), the wave vector of the most unstable wave is equal to ξ_0 (i.e., $\xi^*=1$). The contour plot of ξ^*_{max} for the domains of unstable multilayer growth is shown in Fig. 6. The magnitude of ξ^*_{max} does not significantly vary from 1 except for very small film thicknesses H^*. This implies that in most situations, the wavelength of the interface modulations will be very similar to that for a pure, single-layer film and will not evolve significantly as the multilayer film grows.

The overall stability diagram is a result of the interplay between the three terms in Eq. (10): the surface energy that always favors the smoothing of the surface, the elastic energy relaxation associated with a curved surface, which always favors the growth of surface perturbations, and the contribution from the stress associated with buried interfaces, which may either favor the growth or decay of perturbations. Consider the relatively simple case of the growth of a single layer of material B on the first A layer. When the second layer is very thin, the stress on the surface from the buried A/B interface favors faster B growth in the troughs and slower B growth near the peaks of the surface profile. This, combined with the surface energy term, opposes the elastic energy relaxation term and leads to a decrease in the amplitude of the perturbation of the surface of the second layer. If the buried layer stress effect dominates the surface energy and the atomic mobility is sufficiently high (or the growth rate is sufficiently slow), the second layer will grow from one with perturbations to a nearly flat surface and then, with continued growth, to one for which perturbations of the opposite sign grow. Once perturbations of the opposite sign begin to grow, the elastic energy relaxation term further accelerates their growth. This corresponds to unstable, out-of-phase growth.

The presence of a buried interface may also lead to a different growth mode. As the second layer (B) grows, it may reach the thickness at which the sign of the stress on the surface from the buried interface switches sign [see Eq. (8)]. In this case, the stress from the buried interface favors faster B growth near the peaks on the surface and slower growth near the troughs. This leads to an increase in the amplitude of the perturbation and the layer growth is unstable and in phase, hence the presence of an unstable, in-phase region in the Φ-H^* stability map. The existence of a growing, in-phase surface perturbation will only occur if the atomic mobility (Φ) is sufficiently low that the sign of the surface perturbation does not switch prior to the film thickness achieving the value at which the sign of the stress from the buried interface changes sign. This dependence of the growth mode on the atomic mobility explains the switch from in-phase to out-of-phase growth at large H^* in the Φ-H^* stability map of Fig. 4.

The presence of a region in the stability diagram where the perturbations decay can be understood as a type of out-of-phase growth that did not have sufficient time to be expressed. As discussed above, when the second layer is thin, the stress from the buried layer reinforces the tendency from the surface energy to grow faster in the troughs and slower at the peaks in the surface profile. If given sufficient time, this effect would lead to out-of-phase growth. However, if the growth of the second layer is terminated and the growth of a third layer has begun before the sign of the perturbation switches, the interface is left with a perturbation that is of the same sign but *smaller amplitude* than that of the first interface. This decrease in amplitude of the perturbation upon

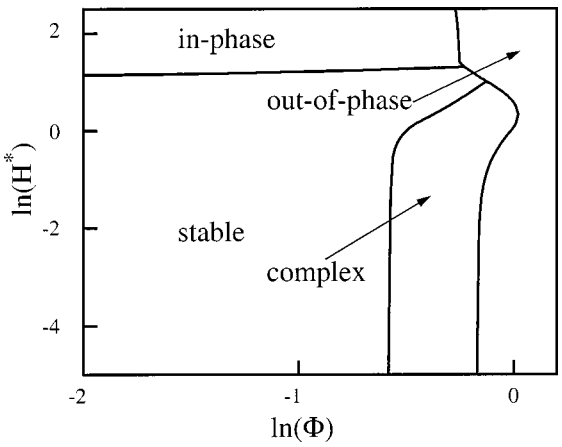

FIG. 7. Stability diagram for a growing multilayer film with a constraint on the wave vector ξ^* to values where an initial perturbation on the first layer would grow (i.e., $\xi^* \leqslant \frac{4}{3}$). This constraint greatly enlarges the region of stable growth (cf. Fig. 4).

growth of an additional layer is the source of the stable region in the multilayer film stability diagram (Fig. 4).

In addition to the in-phase and out-of-phase modes in the unstable regions of the Φ-H^* stability map, there is an unstable domain where the perturbations increase in absolute value but with a sign that is neither always the same nor alternates from layer to layer (i.e., labeled ''complex'' in Fig. 4). This region is between the stable and out-of-phase unstable domains. The origin of this effect cannot be explained on the basis of the two-layer picture used to describe the origin of the other regions of the diagram and is strictly a result of the combined effects of many buried interfaces.

In presenting the stability map (Fig. 4), we tacitly assumed that the wavelength of modulations corresponds to the most unstable wave vector (i.e., that with $\xi^* = \xi^*_{\max}$) and that this perturbation wave vector is constant during the entire growth. However, analysis of the growth of a single-layer film (either pure *A* or pure *B*) showed that perturbations to the surface profile only grow when the wave vector of those perturbations is smaller than a critical value, $\xi < \frac{4}{3}\xi_0$.[4,6] Therefore, there may not be any perturbations available to grow if $\xi^*_{\max} > \frac{4}{3}$. If this is indeed the case, then the stable region of the Φ-H^* stability map will be larger. In order to account for this effect, we reconstruct the stability diagram allowing only wave vectors of magnitude $\xi^*_{\max} \leqslant \frac{4}{3}$. The resultant stability map is presented in Fig. 7. This wave-vector cutoff greatly expands the stable region of the diagram such that the entire small-Φ/small-H^* quadrant is stable. In addition to expanding the stable region of the map, cutting off $\xi^*_{\max}$ greatly expands the unstable region corresponding to the complex eigenvalues.

An additional caveat associated with the present analysis should be kept in mind. Stability or instability in the maps of Figs. 4 and 7 is determined based on how the system will behave in the limit of a large number of layers. The number of layers that must be grown until this analysis is valid is determined by the magnitude of the eigenvalue λ_1 in Eq. (17). Fortunately, the instability develops very quickly over the entire unstable region of Figs. 4 and 7, with the exception of the region near the stable-complex unstable boundary of Fig. 7. Hence, the stability map presented above properly expresses the actual situation under nearly all conditions.

VI. GENERAL CASE

The asymptotic expression for the amplitude of the instability in the general case is derived in the Appendix:

$$\Delta_k^+ = \alpha_1 \Lambda_{11} \lambda_1^{(k-4)/2} \quad \text{and} \quad \Delta_{k-1}^+ = \alpha_1 \Lambda_{12} \lambda_1^{(k-4)/2} \tag{18}$$

for even k, where λ_1 is the maximal eigenvalue and the coefficient α_1 is assumed not negligible compared to the other three expansion coefficients. The matrix Λ is composed of the eigenvectors of matrix $\mathbf{L}$ as defined in the Appendix [see following Eq. (A10)]. The amplitude of the perturbation to the surface on one layer is determined by multiplying the amplitude of the perturbation on the previous layer by $\Lambda_{11}/\Lambda_{12}$ or $\lambda_1 \Lambda_{12}/\Lambda_{11}$ depending on whether the top layer is even or odd. All stability arguments used above to describe the nearly equivalent material case can also be applied to the general case. To be more specific, the eigenvalue λ in the general case corresponds to the square of the same eigenvalue in the nearly equivalent material case and the instability condition $|\lambda| > 1$ applies in the general case as well. The phase of the variation in perturbation amplitude cannot be easily analyzed in the general case because it is determined by both $\Lambda_{11}/\Lambda_{12}$ and $\lambda_1 \Lambda_{12}/\Lambda_{11}$ depending on whether the top layer is even or odd. In the nearly equivalent material case, these two numbers are both equal to the maximal eigenvalue.

Although the dependence of the mode of the perturbation (in phase, out of phase, or complex) on material parameters cannot be easily presented, the question of whether the perturbation is stable or unstable can be easily answered from the analysis of the maximal eigenvalue λ_1. As in the nearly equivalent material case, the overall stability of the structure is determined by whether $|\lambda_1|$ is smaller or larger than unity. Deviation of the materials parameters (misfit stresses, diffusivities, etc.) and the growth conditions from those corresponding to the nearly equivalent material case changes the shape of the region where the multilayer film grows stably (see Fig. 4).

The physical meaning of the eigenvalue λ_1 is how much the amplitude of the instability changes during the growth of a single layer. We can get a sense of how λ_1, for the general case, depends on the material and growth parameters by considering how they would affect the amplitude of the perturbation on the surface of a growing *single*-layer film of material *A* or *B* grown to the thickness of the *A* or *B* layers in the multilayer film:

$$\lambda_A = \exp(\Phi_A H_A^*/2) \quad \text{or} \quad \lambda_B = \exp(\Phi_B H_B^* \beta^8 / 2\Gamma^3). \tag{19}$$

Although the parameters in the expression for λ_B depend explicitly on properties of material *A* due to the normalization employed, the entire expression only depends on the properties of material *B*.

In order to determine how the physical and growth parameters affect the stability of the growing multilayer film, we construct a series of stability diagrams in which we vary the individual physical or growth parameters. Figure 8(a) shows

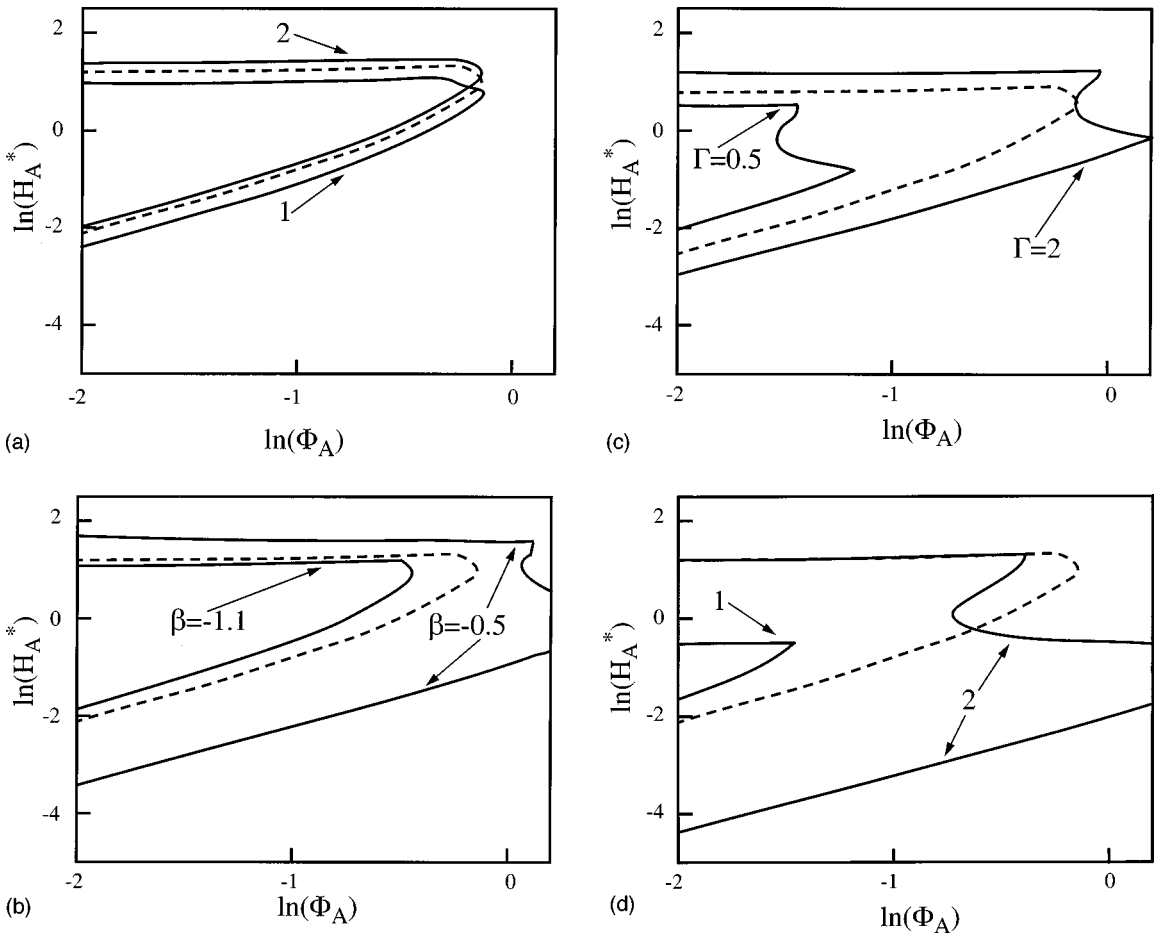

FIG. 8. Stability diagrams for situations where the materials A and B differ from each other by more than simply the sign of the misfit stress. (a) illustrates the influence of relative film thickness. The region of stable growth is bounded by solid curves for $H_A=\frac{2}{3}H_B$ (curve 1) and $H_A=\frac{3}{2}H_B$ (curve 2). (b) illustrates the influence of the relative misfit stress ($\beta=\Sigma_B/\Sigma_A$) for $\Sigma_B=-1.1\Sigma_A$ and $\Sigma_B=-0.5\Sigma_A$. (c) illustrates the influence of the relative surface energy ($\Gamma=\gamma_B/\gamma_A$) for $\gamma_B=0.5\gamma_A$ and $\gamma_B=2\gamma_A$. (d) shows the influence of relative atomic mobility at the growth surface for the case in which $\Phi_A=0.1\,\Phi_B$ (curve 1) and $\Phi_A=10\,\Phi_B$ (curve 2). In all figures, the dashed line shows the boundary between stable and unstable growth for the case where materials A and B are identical except for the sign of the misfit stress. Except where noted, the material parameters and growth conditions in these figures are exactly the same as for Fig. 4.

the stability diagram for the case where the two types of materials are equivalent in every respect except that the thickness of the B layers is either two-thirds or three-halves that of the A layers (and the misfit has opposite sign). The region of stability in this diagram is almost identical to that when the layers have the same thickness (i.e., the nearly equivalent material case—Fig. 4) except for a slight shift in the direction of greater ($H_B=\frac{2}{3}H_A$) or smaller ($H_B=\frac{3}{2}H_A$) layer thickness. This can be qualitatively understood by realizing that a thinner B-layer thickness results in a smaller overall bilayer thickness (i.e., H_A+H_B). In order to achieve the same bilayer thickness, H_A must be increased over that where $H_A=H_B$. This results in an overall shift of the stability in the direction of larger ($H_B=\frac{2}{3}H_A$) or smaller ($H_B=\frac{3}{2}H_A$)H_A, since the superlattice period is plotted against the thickness of layer A. The vertical shift in Fig. 8(a) is approximately equal to the logarithm of the ratio of the bilayer thickness to that when the A and B layers are equal thickness. Changes in the H_A/H_B do not significantly shift the stable region in the Φ_A direction. There is, however, a slight change in the shape of the stable region.

The effect of relative misfit stress on film stability is shown in Fig. 8(b) (other A and B material and growth parameters are identical). For the case where the misfit stress in the B layers is -1.1 times that in the A layers, the domain of stable growth is shifted horizontally (in the $-\ln\Phi_A$ direction) relative to the case where the misfit stress in B is equal to and opposite that in A. When the misfit stress in the B layers is -0.5 times that in A, the domain of stable growth is shifted horizontally, but in the opposite direction (in the $+\ln\Phi_A$ direction) in addition to an overall expansion and the formation of a new nose at large H_A. The shift along the $\ln\Phi_A$ axis may be understood by reference to Eq. (19), where we see that the argument in the exponential is proportional to β^8 (recall that $\beta=\Sigma_B/\Sigma_A$). Increasing β creates an overall increase in the effective value of Φ (i.e., $\Phi_A+\Phi_B\beta^8$). Therefore, the same effective value of Φ is achieved at smaller Φ_A and hence the entire domain of stable growth is shifted toward smaller Φ_A. By the same reasoning, decreasing Φ_B leads to a shift in the domain of stable growth to larger values of Φ_A.

The effect of surface energy on film stability is shown in Fig. 8(c) (other A and B materials and growth parameters are identical, except for misfit which is equal and opposite). In-

creasing the surface energy of material B leads to an overall expansion of the domain of stable growth, while decreasing the surface energy of material B leads to a decrease in the stable domain size. This is opposite to the situation found for the misfit stress, as expected on the basis of Eq. (19). In this case too, the large $\ln\Phi$ peak found when materials A and B are identical (except for the sign of the misfit) breaks into two peaks when the surface energies of the two materials are unequal.

The effect of surface diffusivity on film stability is shown in Fig. 8(d) (other A and B materials and growth parameters are identical, except for misfit which is equal and opposite). Decreasing the surface diffusivity of material B leads to an overall expansion of the domain of stable growth and the splitting of the nose in the domain of stable growth. Increasing the diffusivity of material B leads to shrinking of the stability region in the diagram [Fig. 8(d)]. Interestingly, even though there is an overall expansion of the domain of stable growth in the case where the surface diffusivity of material B is smaller than that of material A, the splitting of the nose results in a portion of the parameter space that was stable when the surface diffusivity of A and B was identical and is unstable when the diffusivity of B is much smaller than that of A. This added complexity makes it difficult to draw general conclusions about the effects that individual material parameters have on multilayer film stability. The change in size of the domain of stable growth can also be understood on the basis of Eq. (19), where the parameter Φ_B is directly proportional to the surface diffusivity. Φ_B is also inversely proportional to the growth rate, such that increasing the growth rate of material B should have the same effect on the stability diagram as decreasing the surface diffusivity.

While we have examined the effects of several material and growth parameters on the stability of multilayer films, some of the parameters may be varied more easily than others. Since surface diffusivity is typically Arrhenius, large variations are possible by changing the temperature with a given system. While all of the other material parameters will likely vary with temperature, these variations are typically small. The largest variations in material parameters will arise when changing the materials that compose the individual layers. Again, the largest variations will typically be found in the surface diffusivity, but changes of order hundreds of percent may be realized in misfit stresses and surface energies as well. On the other hand, the magnitude of variations achievable by changing film thickness is limited by the critical thickness for the formation of misfit dislocations, which is controlled by the magnitude of the misfit. The stability is particularly sensitive to the ratio of misfit stresses and surface energies, which enter Eq. (19) with relatively high powers. Therefore, even though these parameters may not vary as widely as the diffusivity [which enters the exponent in Eq. (19) to the first power], their impact is greater.

In many practical cases of multilayer film growth, the material properties cannot be varied independently. For example, it is often desirable to grow a film under strain-balanced conditions, i.e., where the average stress within the multilayer film is zero. This implies that $H_A\Sigma_A+H_B\Sigma_B=0$. We have examined the effect of varying the misfit stress subject to this constraint. Figure 9 shows the stability diagram for five cases with different ratios of misfit stresses $\beta=\Sigma_B/\Sigma_A$ in the range $-1.1\leqslant\beta\leqslant-0.5$, where the ratio of layer thicknesses H_B/H_A is varied accordingly to keep the multilayer film stress-free (i.e., $H_B/H_A=-1/\beta$). As the absolute value of β increases (β is negative), the domain of stable multilayer growth in the stability diagram shrinks. This is consistent with our observations above [Fig. 8(b)], which showed the same trend with misfit at fixed layer thickness. Increasing the absolute value of β causes a concomitant decrease in H_B/H_A. However, comparing Fig. 9 to Fig. 8(a) (where we vary layer thickness at fixed misfit stresses) shows little correspondence. Therefore, we conclude that variations in layer thickness in order to keep the film stress balanced (zero average stress) are dominated by changes in stress rather than thickness itself. This is consistent with Eq. (19), where we find that stress enters the expression at a much higher power than does layer thickness.

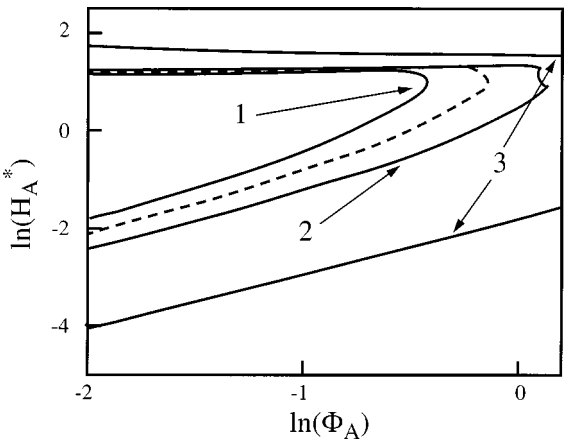

FIG. 9. Stability diagram for the strain-balance superlattice (i.e., superlattices for which $H_A\Sigma_A+H_B\Sigma_B=0$). The dashed curve corresponds to the case where materials A and B differ only by the sign of the misfit stress. The curves labeled 1, 2, and 3 correspond to $\beta=\Sigma_B/\Sigma_A$ equals -1.1, -0.9, and -0.5, respectively (with H_A/H_B adjusted to keep the multilayer film strain-balanced).

Applying the linear stability analysis presented in this study to real experimental systems is a daunting task. A rough estimate of whether the system is in the linear regime during the growth process is determined by the degree to which the eigenvalue λ_1 differs from unity (i.e., the linear theory cannot be reliably applied in cases where $\lambda_1\gg1$). The value of λ_1 can be deduced from the values of λ_A and λ_B [Eq. (19)]. Using the data from Ref. 33 on InAs/AlAs superlattices grown on an InP substrate, and a number of approximations to make up for missing data (such as surface energy of 1 J/m^2), we computed the values of Φ_A and Φ_B using the known values of lattice constants and elastic moduli for the compounds involved as well as the activation energies of surface diffusion.[34] Using these real and estimated data, we find that these experiments correspond to the unstable region of the stability diagram. This is due, in large part, to the very fast surface diffusion of indium atoms. While the formation of interface modulations is consistent with our predictions of an instability, we suspect that the linear stability analysis may be of limited utility in this case since the large value of $\ln\Phi_A$ [$\ln\Phi_A\approx7$ and $\ln H_A^*\approx-3.4$ for experiments reported in Ref. 33 and, as a consequence, the value of λ_A exceeds unity by a few (seven) orders of magnitude] renders the small-

amplitude perturbation assumption of the perturbation theory inapplicable after just a few layers. Determination of the true interface morphology after one or two layers requires use of numerical methods capable of handling strongly nonlinear behavior.[35]

A more tractable system would be GaAs/AlAs superlattices,[36] where the surface diffusivity of Ga is much lower than that of In. However, this system is almost perfectly lattice-matched, which leads to low misfit stresses in the layers. This, combined with the low surface diffusivities of the cations,[34] leads to a prediction that such a film grows stably, as observed in experiments.[36]

Another possibility for testing the linear stability analysis is to turn to superlattices composed of semiconductor alloys rather than of pure III-V compounds. Unfortunately, the presence of two or more alloying elements makes the analysis of surface diffusion complicated and can even introduce new effects.[22] There is a qualitative agreement between the theory presented in this paper and experiments reported in Ref. 12. In that study, multilayer superlattices of $InAs_yP_{1-y}/Ga_{1-x}In_xP$ were grown. The morphology of the films observed in these experiments, observed using transmission electron microscopy, shows both morphological and compositional modulations of the structure which can be classified as out-of-phase unstable growth.

VII. CONCLUSIONS

In the present analysis, we focused primarily on the special case of a multilayer film, where the materials parameters and growth conditions of the two types of layers are identical, with the exception that the misfit stresses are equal and opposite. Our findings are reported in the form of stability diagrams in the plane defined by the two key parameters: layer thickness and normalized surface diffusivity. We found that, unlike the case of a thin film consisting of a single layer, there are conditions under which the film is stable, i.e., perturbations to the growth surface decay. For the regions of unstable film growth (where the amplitude of the perturbation grows from layer to layer), we distinguish three different types of resulting film morphology, classified according to the complex phase of the characteristic number λ, which is a function of materials parameters and growth conditions. Positive λ corresponds to the ''in-phase'' perturbation growth mode where perturbations at all interfaces are in phase. Negative λ corresponds to the ''out-of-phase'' growth mode where the perturbations at consecutive interfaces are phase-shifted by a half-wave with respect to one another. This leads to a form of lateral composition modulation. A case corresponding to λ which possesses a nonzero imaginary part is characterized by an irregular sign shift between perturbations at consecutive layer interfaces, which is determined by the complex phase of λ. We also determined the wave vector of the propagating perturbation corresponding to the fastest growing instability wave and the rate of perturbation growth.

We also considered the general case in which the two materials and the film growth conditions can vary. We explicitly examined how the surface diffusivity of the two materials, growth rate, surface energy, and film thickness affect the stable domain in the stability diagram. In short, we found that changing the thickness of one layer shifts the stable growth region in the stability diagram, but primarily because it changes the average layer thickness. The boundary of the domain of stable growth is approximately the same, for a given superlattice period (sum of layer thicknesses), whether the individual layers have the same or slightly different thicknesses.

Increasing the surface diffusivity or, alternatively, decreasing the deposition rate of one of the layers shrinks the stable growth region in the stability diagram. Increasing the magnitude of the misfit stress or decreasing the surface energy produces a similar overall effect; qualitative details of the influence of each of the materials parameter can be understood through consideration of how the parameter modifies λ.

ACKNOWLEDGMENTS

The authors would like to thank Professor J. R. Barber, Professor R. S. Goldman, and Professor J. Mirecki-Millunchick for useful discussions. D.F.S. gratefully acknowledges the support of the U.S. Department of Energy, Grant No. DE-FG02-99ER45797.

APPENDIX: SOLUTION OF THE RECURRENCE RELATIONS

In this appendix, we obtain closed-form solutions to the evolution equations for the surface of the growing multilayer film. As in the main text, we first consider the special case where materials *A* and *B* are identical in every respect, except that the magnitude of the misfit stress Σ with respect to the substrate is equal and opposite in the two materials (i.e., $\beta=-1$). In this case, the integration of the evolution equation resulted in two expressions [Eqs. (14′) and (12′)]:

$$X_k = X_{k-1}F - 2\sum_{j=1}^{k-1}(-1)^{k-j-1}X_j[\Psi H^*(k-j-1)+\Xi] \tag{A1}$$

and

$$X_j = \Delta_j e^{\xi^* H^*(j-1)} \tag{A2}$$

from which the amplitude of the perturbation Δ_k of layer k can be found using successive iterations. This recurrence relation can be greatly simplified by rewriting Eq. (A1) as

$$X_{k+3} = X_{k+2}(F-2-2\Xi) + X_{k+1}(2F-1+2\Psi H^*-2\Xi) + X_k F, \tag{A3}$$

which only involves four consecutive terms. Applying Eq. (A2) to the previous relation produces a recurrence relation for Δ_k:

$$\Delta_{k+3} = \Delta_{k+2}e^{-\xi^* H^*}(F-2-2\Xi) + \Delta_{k+1}e^{-2\xi^* H^*} \times (2F-1+2\Psi H^*-2\Xi) + \Delta_k e^{-3\xi^* H^*}F. \tag{A4}$$

As in the text, we normalize the amplitudes of the perturbation Δ_k by Δ_1: $\Delta_k^+ = \Delta_k/\Delta_1$. The perturbation amplitude Δ_k^+ can be rewritten in closed form in terms of a power of the 3×3 matrix $\mathbf{L}$:

$$\mathbf{L} = \begin{pmatrix} e^{-\xi^* H^*}(F-2-2\Xi) & 1 & 0 \\ e^{-2\xi^* H^*}(2F-1+2\Psi H^*-2\Xi) & 0 & 1 \\ e^{-3\xi^* H^*}F & 0 & 0 \end{pmatrix}. \tag{A5}$$

The perturbation amplitudes for three consecutive layers can be expressed as vectors $\mathbf{Y}_k$: $\mathbf{Y}_k = \langle \Delta_{k+2}^+, \Delta_{k+1}^+, \Delta_k^+ \rangle$. The vector $\mathbf{Y}_k$ is related to the vector $\mathbf{Y}_1$ by the $(k-1)$th power of matrix $\mathbf{L}$: $\mathbf{Y}_k = \langle \Delta_{k+2}^+, \Delta_{k+1}^+, \Delta_k^+ \rangle = \mathbf{Y}_1 \mathbf{L}^{k-1} = \langle \Delta_3^+, \Delta_2^+, \Delta_1^+ \rangle \mathbf{L}^{k-1}$. Finding the values of Δ_2 and Δ_3 using Eqs. (12′), (14′) and arbitrary Δ_1 determines the vector $\mathbf{Y}_1$. Applying the matrix $\mathbf{L}$ to this vector $k-1$ times determines the amplitude Δ_k^+.

The power of the matrix grows as fast as the power of its eigenvalues. We denote the three eigenvalues of the matrix $\mathbf{L}$ as λ_1, λ_2, and λ_3. Assuming that $\mathbf{L}$ is not degenerate, we express the matrix of eigenvectors Λ of matrix $\mathbf{L}$ as

$$\mathbf{\Lambda} = \begin{pmatrix} \lambda_1^2 & \lambda_1 & 1 \\ \lambda_2^2 & \lambda_2 & 1 \\ \lambda_3^2 & \lambda_3 & 1 \end{pmatrix}. \tag{A6}$$

The expression for Δ_k^+ $(k \geqslant 4)$ can now be written as

$$\Delta_k^+ = \alpha_1 \lambda_1^{(k-1)} + \alpha_2 \lambda_2^{k-1} + \alpha_3 \lambda_3^{k-1}, \tag{A7}$$

where the α's are the coefficients of the expansion of vector $\mathbf{Y}_1$ in the basis of the eigenvectors of matrix $\mathbf{L}$: $\langle \alpha_1, \alpha_2, \alpha_3 \rangle = \mathbf{Y}_1 \mathbf{\Lambda}^{-1} = \langle \Delta_3^+, \Delta_2^+, 1 \rangle \mathbf{\Lambda}^{-1}$. Δ_k^+ grows asymptotically as the power of the maximal eigenvalue of matrix $\mathbf{L}$. Because of this power law, the asymptotic regime is reached quickly, provided that the coefficient α_i corresponding to that maximal eigenvalue of $\mathbf{L}$ (denoted λ_1) is not much smaller than the other two α's.

We now turn to the general case [Eqs. (12) and (14)], where materials A and B may be different. It is possible to derive a recurrence relation similar to Eq. (A4), in terms of two 4×4 matrices, one each for the odd- and even-numbered layers. In particular, we find

$$\begin{aligned} X_{k+4} = {} & X_{k+3}\left[F_B + \beta(1-\beta)\Xi_B + \frac{\Psi_B}{\Psi_A}\beta \right] \\ & + X_{k+2}\left[1 - \beta(1-\beta)\left(\Xi_B + \Psi_B H_A^* - \frac{\Psi_B}{\Psi_A}\Xi_A \right) \right. \\ & \left. - \frac{\Psi_B}{\Psi_A}\beta F_A \right] - X_{k+1}\left[F_B + \frac{\Psi_B}{\Psi_A}\beta \right. \\ & \left. + \beta(1-\beta)\left(\frac{\Psi_B}{\Psi_A}\Xi_A - \Psi_B H_A^* \right) \right] + X_k\left[\frac{\Psi_B}{\Psi_A}\beta F_A \right] \end{aligned} \tag{A8a}$$

for even k and

$$\begin{aligned} X_{k+4} = {} & X_{k+3}\left[F_A - (1-\beta)\Xi_A + \frac{\Psi_A}{\Psi_B\beta} \right] \\ & + X_{k+2}\left[(1-\beta)\left(\Xi_A + \Psi_A H_B^* - \frac{\Psi_A}{\Psi_B}\Xi_B \right) \right. \\ & \left. + 1 - F_B\frac{\Psi_A}{\Psi_B\beta} \right] - X_{k+1}\left[(1-\beta)\left(\Psi_A H_B^* - \frac{\Psi_A}{\Psi_B}\Xi_B \right) \right. \\ & \left. + F_A + \frac{\Psi_A}{\Psi_B\beta} \right] + X_k\left[F_B\frac{\Psi_A}{\Psi_B\beta} \right] \end{aligned} \tag{A8b}$$

for odd k. We use Eq. (12) to obtain similar relations for Δ_k or Δ_k^+. We define the two 4×4 matrices $\mathbf{L}_A$ and $\mathbf{L}_B$:

$$\mathbf{L}_A = \begin{pmatrix} L_A^{11} & 1 & 0 & 0 \\ L_A^{21} & 0 & 1 & 0 \\ L_A^{31} & 0 & 0 & 1 \\ L_A^{41} & 0 & 0 & 0 \end{pmatrix}, \quad \mathbf{L}_B = \begin{pmatrix} L_B^{11} & 1 & 0 & 0 \\ L_B^{21} & 0 & 1 & 0 \\ L_B^{31} & 0 & 0 & 1 \\ L_B^{41} & 0 & 0 & 0 \end{pmatrix}. \tag{A9}$$

The matrix coefficients $\mathbf{L}_A^{i1}$ are simply the product of the ith bracketed term in Eq. (A8a) and $e^{-\xi^*\eta_i}$, where η_i is H_A^*, $H_A^*+H_B^*$, $2H_A^*+H_B^*$, and $2(H_A^*+H_B^*)$ for $i=1$, 2, 3, and 4, respectively. Similarly, the matrix coefficients $\mathbf{L}_B^{i1}$ are simply the product of the ith bracketed term in Eq. (A8b) and $e^{-\xi^*\eta_i}$, where η_i is H_B^*, $H_A^*+H_B^*$, $H_A^*+2H_B^*$, and $2(H_A^*+H_B^*)$ for $i=1$, 2, 3, and 4, respectively.

In the general case, the vector $\mathbf{Y}_k$ has four components $\mathbf{Y}_k = \langle \Delta_{k+3}^+, \Delta_{k+2}^+, \Delta_{k+1}^+, \Delta_k^+ \rangle$. The amplitude of the vector $\mathbf{Y}_k$ is simply

$$\mathbf{Y}_k = \mathbf{Y}_1(\mathbf{L}_B\mathbf{L}_A)^{(k-1)/2} = \langle \Delta_4^+, \Delta_3^+, \Delta_2^+, 1 \rangle (\mathbf{L}_B\mathbf{L}_A)^{(k-1)/2} \tag{A10}$$

for odd values of k and $\mathbf{L}_A$ times this for even values of k. Defining the matrix $\mathbf{L}$ as a product of matrices $\mathbf{L}_B$ and $\mathbf{L}_A$ and the matrix Λ as the matrix of the eigenvectors of matrix $\mathbf{L}$ corresponding to the eigenvalues λ_1, λ_2, λ_3, and λ_4, we obtain a closed-form expression for Δ_k^+. Assuming that k is even and is greater than 4, we have

$$\Delta_k^+ = \sum_{i=1}^{4} \alpha_i \Lambda_{i1} \lambda_i^{(k-4)/2} \quad \text{and} \quad \Delta_{k-1}^+ = \sum_{i=1}^{4} \alpha_i \Lambda_{i2} \lambda_i^{(k-4)/2}, \tag{A11}$$

where Λ_1 and Λ_2 are the components of the first and second column of the matrix of the eigenvectors of Λ, respectively, and α is the expansion coefficient of the vector in the basis of eigenvectors: $\langle \alpha_1, \alpha_2, \alpha_3, \alpha_4 \rangle = \mathbf{Y}_1 \mathbf{\Lambda}^{-1}$.

As in the case of nearly equivalent materials A and B, when the materials in these layers are different we only need to consider the asymptotic part of Eqs. (A11), i.e.,

$$\Delta_k^+ = \alpha_1 \Lambda_{11} \lambda_1^{(k-4)/2} \quad \text{and} \quad \Delta_{k-1}^+ = \alpha_1 \Lambda_{12} \lambda_1^{(k-4)/2}, \tag{A12}$$

where λ_1 is the maximal eigenvalue. All of the stability arguments used in the nearly equivalent layers case can be applied to the general case. To be more specific, the eigenvalue λ, in the general case, corresponds to the square of the

same eigenvalue in the nearly equivalent layers case and the instability condition $\lambda_1 > 1$ applies in the general case as well. The phase of the perturbation cannot be easily analyzed because the phase between two successive layers is now determined by two numbers: $\Lambda_{11}/\Lambda_{12}$ if we proceed from an odd-numbered layer to an even-numbered one and $\lambda_1\Lambda_{12}/\Lambda_{11}$ if we proceed from an even-numbered layer to an odd-numbered one. In the nearly equivalent layers case, these two values are equal to each other.

Although the dependence of the mode of the perturbation of the growth conditions and material parameters cannot be easily presented for the general case, the question of whether the perturbation is stable or unstable can be easily answered from the analysis of the maximal eigenvalue λ_1.

[1] J. W. Matthews and A. E. Blakeslee, J. Cryst. Growth **32**, 265 (1976).
[2] D. C. Houghton, D. D. Perovic, J.-M. Baribeau, and G. C. Weatherly, J. Appl. Phys. **67**, 1850 (1990).
[3] J. P. Hirth and X. Feng, J. Appl. Phys. **67**, 3343 (1990).
[4] R. J. Asaro and W. A. Tiller, Metall. Trans. **3**, 1789 (1972).
[5] M. A. Grinfeld, Dokl. Akad. Nauk **10**, 1358 (1986) [Sov. Phys. Dokl. **31**, 831 (1986)].
[6] D. J. Srolovitz, Acta Metall. **37**, 621 (1989).
[7] A. J. Pidduck, D. J. Robbins, A. G. Cullis, W. Y. Leong, and A. M. Pitt, Thin Solid Films **222**, 78 (1992).
[8] D. E. Jesson, S. J. Pennycook, J.-M. Baribeau, and D. C. Houghton, Phys. Rev. Lett. **71**, 1744 (1993).
[9] C. S. Ozkan, W. D. Nix, and H. Gao, Appl. Phys. Lett. **70**, 2247 (1997).
[10] K. C. Hsieh, J. N. Baillargeon, and K. Y. Cheng, Appl. Phys. Lett. **57**, 2244 (1990).
[11] K. Y. Cheng, K. C. Hsieh, and I. N. Baillargeon, Appl. Phys. Lett. **60**, 2892 (1992).
[12] A. Ponchet, A. Rocher, A. Ougazzaden, and A. Mircea, J. Appl. Phys. **75**, 7881 (1994).
[13] S. T. Chou, K. Y. Cheng, L. J. Chou, and K. C. Hsieh, J. Appl. Phys. **78**, 6270 (1995).
[14] J. Mirecki-Millunchick, R. D. Twesten, D. M. Follstaedt, S. R. Lee, E. D. Jones, Y. Zhang, S. P. Ahrenkiel, and A. Mascarenhas, Appl. Phys. Lett. **70**, 1402 (1997).
[15] N. Y. Jin-Phillipp, F. Phillipp, T. Marschner, and W. Stolz, J. Mater. Sci.: Mater. Electron. **8**, 289 (1997).
[16] J. Tersoff, C. Teichert, and M. G. Lagally, Phys. Rev. Lett. **76**, 1675 (1996).
[17] D. Leonard, M. Krishnamurthy, C. M. Reaves, S. P. Denbaars, and P. M. Petroff, Appl. Phys. Lett. **63**, 3203 (1993).
[18] D. J. Eagelsham and M. Cerullo, Phys. Rev. Lett. **64**, 1943 (1990).
[19] N. N. Ledentsov, V. M. Ustinov, V. A. Shchukin, P. S. Kop'ev, Zh. I. Alferov, and D. Bimberg, Semiconductors **32**, 343 (1998).
[20] B. J. Spencer, P. W. Voorhees, and S. H. Davis, J. Appl. Phys. **73**, 4955 (1993).
[21] J. Tersoff, Phys. Rev. B **56**, R4394 (1997).
[22] P. Venezuela and J. Tersoff, Phys. Rev. B **58**, 10 871 (1998).
[23] J. E. Guyer and P. W. Voorhees, J. Cryst. Growth **187**, 150 (1998).
[24] F. Glas, Appl. Surf. Sci. **123/124**, 298 (1998).
[25] I. P. Ipatova, V. G. Malyshkin, A. A. Maradudin, V. A. Shchukin, and F. Wallis, Phys. Rev. B **57**, 12 968 (1998).
[26] F. Leonard and R. C. Desai, Phys. Rev. B **57**, 4805 (1998).
[27] P. H. Leo and R. F. Sekerka, Acta Metall. **37**, 3119 (1989).
[28] W. W. Mullins, J. Appl. Phys. **28**, 333 (1957).
[29] V. A. Shchukin, D. Bimberg, V. G. Malyshkin, and N. N. Ledentsov, Phys. Rev. B **57**, 12 262 (1998).
[30] G. Springholz, V. Holy, M. Pinczolits, and G. Bauer, Science **282**, 5389 (1998).
[31] J. D. Eshelby, Proc. R. Soc. London, Ser. A **241**, 376 (1957).
[32] C. Teodosiu, *Elastic Models of Crystal Defects* (Springer-Verlag, Berlin, 1982).
[33] S. P. Ahrenkiel, A. G. Norman, M. M. Al-Jassim, A. Mascarenhas, J. Mirecki-Millunchick, R. D. Twesten, S. R. Lee, D. M. Follstaedt, and E. D. Jones, J. Appl. Phys. **84**, 6088 (1998).
[34] T. Shitara, D. D. Vvedensky, J. H. Neave, and B. A. Joyce, in *Common Themes and Mechanisms of Epitaxial Growth Symposium*, edited by P. Fuoss, J. Tsao, D. W. Kisker, A. Zangwill, and T. Kuech (Materials Research Society, Pittsburgh, 1993), Vol. 312, p. 267.
[35] B. J. Spencer and D. I. Meiron, Acta Metall. Mater. **42**, 3629 (1994).
[36] Y. Hsu, W. I. Wang, and T. S. Kuan, J. Vac. Sci. Technol. B **14**, 2286 (1996).